Rapid Active Power Control of Photovoltaic Systems for Grid Frequency Support

Anderson F. Hoke, *Member, IEEE*, Mariko Shirazi, *Member, IEEE*, Sudipta Chakraborty, *Senior Member, IEEE*, Eduard Muljadi, *Fellow, IEEE*, and Dragan Maksimovic, *Fellow, IEEE*

***Abstract*— As deployment of power electronic coupled generation such as photovoltaic (PV) systems increases, grid operators have shown increasing interest in calling on inverter-coupled generation to help mitigate frequency contingency events by rapidly surging active power into the grid. When responding to contingency events, the faster the active power is provided, the more effective it may be for arresting the frequency event. This paper proposes a predictive PV inverter control method for very fast and accurate control of active power. This rapid active power control (RAPC) method will increase the effectiveness of various higher-level controls designed to mitigate grid frequency contingency events, including fast power-frequency droop, inertia emulation, and fast frequency response, without the need for energy storage. The RAPC method, coupled with a maximum power point estimation method, is implemented in a prototype PV inverter connected to a PV array. The prototype inverter's response to various frequency events is experimentally confirmed to be fast (beginning within 2 line cycles and completing within 4.5 line cycles of a severe test event) and accurate (below 2% steady-state error).**

***Index Terms*— Active power control (APC), frequency control, inverters, photovoltaics (PVs), power systems.**

I. Introduction

As THE portion of electricity that is produced by solar photovoltaic (PV) systems increases, it is increasingly required that PV systems provide many of the grid support functions that are traditionally performed by conventional rotating machines. One of the most crucial frequency support needs is for response to contingency events [1], however, state-of-the-art PV systems typically do not provide this service. Frequency contingency events—especially those on low-inertia grids—require a very fast injection of power into the grid to arrest falling frequency; the faster the response, the more valuable it may be for frequency stabilization [2], [3]. For example, the Hawaiian Electric Companies have proposed a fast frequency regulation (FFR) service with a "total reaction time" of six line cycles, or 100 ms [4]. Conventional PV active power control (APC) methods are significantly faster than synchronous machine governor controls but significantly slower that synchronous machine inertial response, and certainly slower than 100 ms [5]. This is partly because there has been little motivation in the past for PV inverters to modulate power on subsecond time scales, so typical APCs [e.g., maximum power point tracking (MPPT)] are not necessarily designed for subsecond response times. This paper proposes an accurate method of rapid APC (RAPC) of PV systems that achieves response times approaching inertial-response time-scales, thus enabling highly effective contingency event mitigation.

It is becoming standard for PV inverters to be able to control reactive power for voltage support, to ride through transient voltage and frequency events, and to curtail active power during times of high-grid frequency [6], [7]. Some electric power system operators are also requiring large PV generators to provide primary frequency regulation [8], [9], a requirement that is typically addressed by incorporating energy storage. However, current storage technologies have shorter lifetimes than other PV system components, and while battery costs are falling, they have not seen the dramatic reductions that PV modules have [10]. Thus it may be desirable for PV systems to provide some degree of both up- and down-regulating active power modulation in high-penetration applications without the need for energy storage. The term "bidirectional APC" is used here to mean that the PV output power can be modulated both up and down (but not that net active power is absorbed).

Bidirectional APC of a PV system requires operating below the MPP of the system and thus incurs an opportunity cost; hence it has historically been of little interest for grid-interactive PV system operators. However, in scenarios with very high renewable energy penetration, bidirectional APC of PV is increasingly of interest [5], [9], [11], [12]. In addition, in some power systems such as the California ISO, PV plants are already curtailed at times and hence could provide APC services without incurring opportunity cost. PV systems without storage can of course only provide APC services within the limitations of the input solar power availability. However, with PV generation on some grids reaching 50% or more of instantaneous generation at times [13], the need for APC rises. At times when PV generation is low or zero,

Manuscript received October 6, 2016; revised December 19, 2016 and February 2, 2017; accepted February 7, 2017. Date of publication February 20, 2017; date of current version July 31, 2017. This work was supported in part by the U.S. Department of Energy under Contract DE-AC36-08-GO28308 with the National Renewable Energy Laboratory. This paper was recommended for publication by Associate Editor Carl N. M. Ho.

A. F. Hoke was with the Electrical, Computer, and Energy Engineering Department, University of Colorado, Boulder, CO 80309 USA. He is now with the Power Systems Engineering Center, National Renewable Energy Laboratory, Golden, CO 80401 USA (e-mail: andy.hoke@nrel.gov).

M. Shirazi, S. Chakraborty, and E. Muljadi are with the Power Systems Engineering Center, National Renewable Energy Laboratory, Golden, CO 80401 USA.

D. Maksimovic is with the Electrical, Computer, and Energy Engineering Department, University of Colorado, Boulder, CO 80309 USA (e-mail: maksimov@colorado.edu).

Color versions of one or more of the figures in this paper are available online at http://ieeexplore.ieee.org.

Digital Object Identifier 10.1109/JESTPE.2017.2669299

greater amounts of other generation are online and can be called upon to provide active power services.

Development of APCs for grid-interactive PV systems for frequency support and other purposes is progressing, but is still at an early technology readiness level [5], [11]. A number of past works have proposed various APC methods for grid-connected PV systems. In [14], some methods for improved APC of distributed generation during grid faults are described; these methods focus on maintaining stable active power output during unbalanced voltage conditions and are not intended for rapidly finding the new PV array dc operating point needed for a desired adjustment in active power. In [15], a fuzzy logic controller is used to regulate the frequency of a PV-diesel-battery microgrid, and it is noted that the battery system could be removed if the PV plant were operated below MPP. In [16], it is proposed that a power reserve be provided by operating a PV array below its open circuit voltage by a set percentage. Droop control is proposed in [17] and [18] to regulate frequency using PV inverters, but the effects of changing irradiance and temperature are not accounted for. A simulation of a PV system providing emulated inertial response with constant irradiance is presented in [19]. In [20], a PV inverter connected to a PV simulator is used to provide primary frequency response, but inverter control details are not provided. An adaptive droop control method for PV microgrid frequency regulation is proposed in [21]. A method for estimating the maximum power available from a PV array without measuring irradiance, assuming a constant maximum power voltage, has been proposed in [22]. And recently, a large-scale field demonstration of a PV plant providing primary and secondary frequency regulation represented a major step forward in the development of PV APC [5]. The following two key areas for improvement are noted in [5]:

1) a need for accurate online estimation of the maximum power available from a PV array when not operating at MPP;
2) a potential for faster APC response from more optimal controls.

The first item can be addressed by an online MPP estimation (MPPE) method proposed in [23] and validated in hardware for the first time in Section II (though other methods are also emerging [22]). The second item can be addressed by the RAPC method presented in Section III and validated experimentally in Section IV. A key challenge addressed by the RAPC method is the need to modulate PV system output power to a desired level by adaptively controlling PV array voltage in the presence of continuous weather-induced changes in the array's current-voltage characteristic. Because rapidly modulating the output of a grid-interactive PV inverter to a new power level has not historically been of interest, there is little existing research on this topic.

While the RAPC method is the primary new contribution of this paper, the MPPE method is summarized first because the two methods are closely related and can be used in conjunction to enable fast and accurate frequency support from PV inverters. To be clear, the MPPE method is not intended as a substitute for MPPT, but rather as a way of estimating the available array power while not operating at the MPP, a challenging task [24]. Together, MPPE and RAPC enable very fast PV response to frequency events via any of a number of existing control methods including but not limited to power-frequency droop control [25], inertia emulation [26], or FFR (a new grid service under consideration in the ERCOT interconnection and elsewhere) [27]. The scope of this paper does not include grid voltage support techniques as these are already well documented in the literature, for example, in [6], [28], and [29].

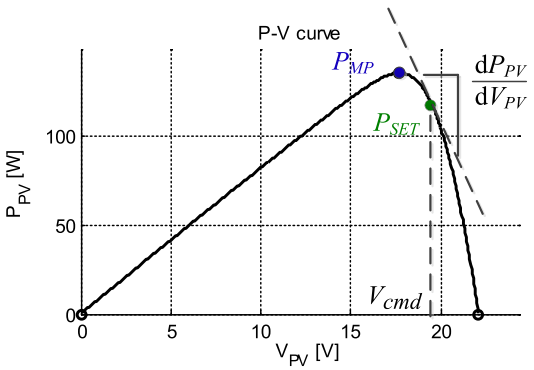

Fig. 1. Sample power-voltage curve of a single PV module.

Both the RAPC method and the MPPE method have the advantage that they can be implemented in a PV inverter controller using information generated once (e.g., at the time of commissioning) through offline calculations starting from typical PV module data sheet parameters.

II. Online Maximum Power Point Estimation

The output power of a PV system, P_{PV}, is a nonlinear function of the operating voltage of the PV array, V_{PV}. The challenge of fast and accurate large-signal PV APC is that the PV array power-voltage curve, an example of which is shown in Fig. 1, is constantly changing throughout a wide range as solar irradiance and PV module temperature vary, so the maximum power P_{MP} is not generally known. Typically, current-controlled PV inverters use one of a variety of MPPT methods, such as perturb and observe, to regulate output power to P_{MP} [30], [31]. Typical MPPT methods rely on actually operating near P_{MP} to determine P_{MP}. To provide the necessary power headroom for APC while minimizing the opportunity cost of operating below P_{MP}, an accurate real-time estimate of P_{MP} is needed.

Both the MPPE method and the RAPC method presented here assume that the PV array is not partially shaded or otherwise nonuniform, so array voltages and currents can be calculated by scaling according to the total number of cells in series and in parallel, respectively. This approximation is good but not perfect for typical PV arrays. When implementing an APC scheme, small errors due to nonuniformity can be accounted for by increasing the reserve power by a small margin to ensure that the desired reserve power P_{RES} is available under worst case expected error conditions. For PV systems that regularly experience significant partial shading, the MPPE and RAPC methods proposed here are not appropriate; developing methods appropriate for shaded systems is a topic for future work.

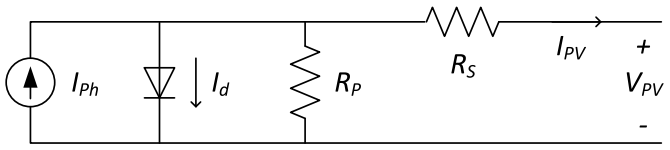

Fig. 2. Five-parameter model of a PV cell.

A. MPPE Method

The current-voltage (I–V) and power-voltage curves of a PV array are determined by the irradiance, G, incident on the array and by the PV cell temperature, T. The I–V curve can be well-approximated using a five-parameter PV cell model [32] shown in Fig. 2 and described in the following:

$$\begin{aligned} I_{\rm PV} &= I_{\rm Ph}(G,T) - I_0(G,T)\left(e^{\left(\frac{q(V_{\rm PV}+R_S I_{\rm PV})}{knT}\right)} - 1\right) \\ &\quad - \frac{V_{\rm PV} + R_S I_{\rm PV}}{R_P} \\ I_{\rm Ph} &= \frac{G}{G_{\rm STC}} I_{\rm SC}\left(\frac{R_S + R_P}{R_P}\right)(1 + K_I(T - T_{\rm STC})) \\ I_0 &= \frac{I_{\rm Ph} - V_{\rm OC}/R_P}{e^{\left(\frac{qV_{\rm OC}}{knT}\right)} - 1}. \end{aligned} \tag{1}$$

Here, $I_{\rm PV}$ is the net PV cell current, $I_{\rm Ph}$ is the light-generated photocurrent, I_0 is the diode saturation current of the PV cell p-n junction, q is the electron charge, $V_{\rm PV}$ is the PV cell voltage, R_S is the modeled series resistance, k is Boltzmann's constant, n is the diode ideality constant (assumed to be $n = 1$, as in [32]), R_P is the modeled shunt resistance, $G_{\rm STC} = 1000$ W/m^2 is the irradiance at standard test conditions (STC), $I_{\rm SC}$ is the data sheet short-circuit current (at STC), K_I is the data sheet temperature coefficient of $I_{\rm SC}$, $T_{\rm STC} = 25$ °C is the temperature at STC, and $V_{\rm OC}$ is the data sheet open-circuit voltage (at STC).

However, even with known irradiance and cell temperatures, solving the P–V curve is computationally intensive due to the need to solve the transcendental implicit equation (1) [33]. In addition, R_S and R_P are not given in PV module or cell data sheets. Thus, solving (1) rapidly in real time in an embedded processor is a difficult task, as is finding the MPP $P_{\rm mp1} = \max(I_{\rm PV}(G,T)^* V_{\rm PV}(G,T))$. The MPPE method presented here avoids those tasks by solving the entire operating space $P_{\rm mp1} = f(G,T)$ beforehand and using linear regression to derive a second-order polynomial that predicts $P_{\rm mp1}(G,T)$

$$P_{\rm mp1} = d + a_1 T + a_2 T^2 + b_1 G + b_2 G^2 + cTG. \tag{2}$$

All lowercase letters in (2) are regression coefficients. Fig. 3 shows a flowchart of the process used to find the regression coefficients in (2). Calculation details and an example calculation are provided in [23]. Briefly, the first step involves using Villalva's method [32] to find R_S and R_P from data sheet parameters. Step 2 then numerically solves for $I_{\rm PV}$ over the entire ($V_{\rm PV}$, G, T) operating space (where $\mathbf{X}$ is a vector of (G,T) pairs covering the expected operating conditions). Step 3 finds the maximum PV array power $\mathbf{P_{mp1}(X)}$, again for all expected operating conditions. Finally, Step 4 uses linear regression of the $\mathbf{P_{mp1}(X)}$ data to find the polynomial coefficients for (2).

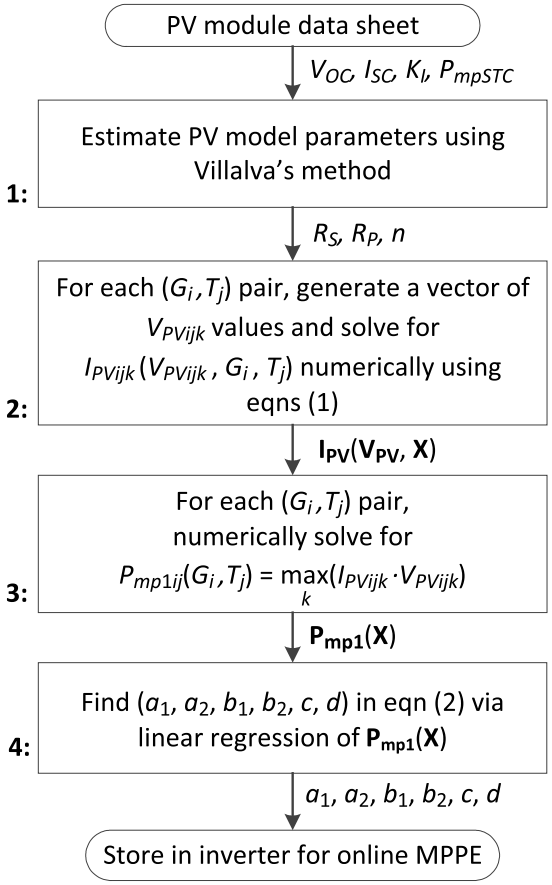

Fig. 3. Flowchart for offline calculation of MPPE parameters in (2).

The calculation process illustrated in Fig. 3 only needs to be performed once for each PV system, and it is performed offline on a standard computer. The regression coefficients are then stored in the PV inverter controller's on-board memory for use in real-time MPPE. The coefficient of determination ("R squared") of the regression fit is typically very high, e.g., 0.999, where 1.0 indicates a perfect fit, indicating that the second order polynomial provides a very accurate prediction [23].

Because the process shown in Fig. 3 is performed for a single PV module, the estimated system ac output power can be calculated as $P_{\rm MPPE} = P_{\rm mp1}(G,T) \cdot N \cdot \eta$, where N is the number of modules in the array and η is the conversion efficiency of the PV plant.

The output power of PV modules degrades over their lifetime. This degradation is fairly linear with time and typically proceeds at a rate of less than 1% per year, with 0.5% per year being typical [34]. Degradation can be accounted for in MPPE by modifying the system conversion efficiency, η, as a function of time, t, in days since the system was installed

$$\eta = \eta_0 \cdot \left(1 - \frac{r \cdot t}{365}\right). \tag{3}$$

Here r is the annual rate of degradation of $P_{\rm MP}$ and η_0 is the total conversion efficiency of the PV system at the time of installation, which can be determined experimentally during commissioning or estimated from system component specifications.

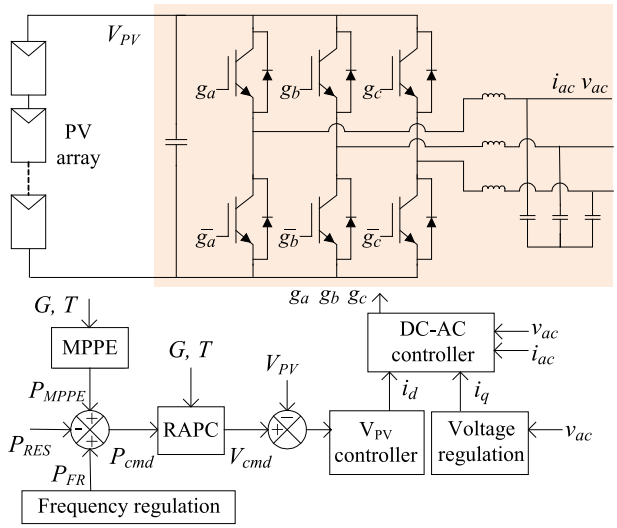

Fig. 4. Inverter for hardware validation of MPPE and RAPC.

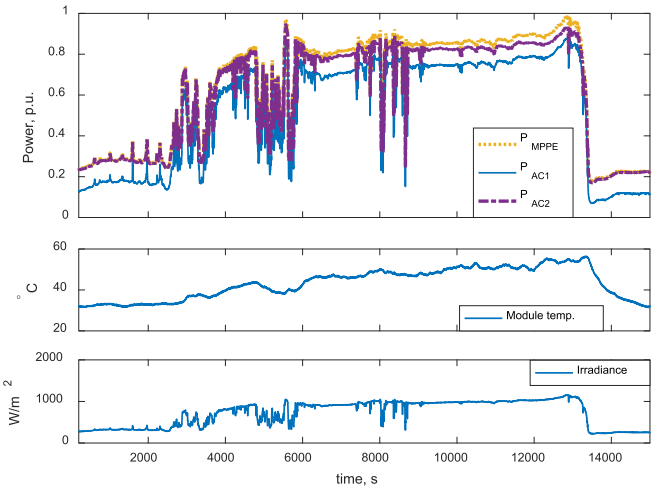

Fig. 5. Prototype inverter operating in MPPE mode with 500 W of reserve power while another inverter operates in MPPT mode.

B. MPPE Experimental Validation

For demonstration purposes, the MPPE method was implemented in a three-phase, single-stage prototype inverter using a simple three-phase bridge power stage and an L-C output filter, as shown in Fig. 4. However, the MPPE method, like the RAPC method described in Section III, is not topology-specific: both can be used with a wide range of inverter topologies and low-level control schemes, such as those described in [35]–[37].

The low level controls of the prototype inverter were implemented in the field-programmable gate array of a National Instruments sbRIO controller [38], and the MPPE (and RAPC) controls were implemented in the sbRIO's real-time processor. The MPPE block calculates the estimated the available power P_{MPPE} as described above. The power reserve P_{RES} should be provided by grid-level controls based on anticipated needs for up-regulation; the inverter-level controls described here take P_{RES} as an external input. The frequency regulation block provides the required change in output power needed to respond to a frequency event, P_{FR}. In the RAPC demonstration provided in Section IV, the frequency regulation block implements a simple power-frequency droop response as in [11]. The power command P_{cmd} is equal to $P_{\mathrm{MPPE}} - P_{\mathrm{RES}} + P_{\mathrm{FR}}$. In the absence of a frequency event P_{FR} is zero, so the inverter simply operates at $P_{\mathrm{cmd}} = P_{\mathrm{SET}}$, maintaining a reserve power equal to P_{RES} available for up-regulation. The RAPC block converts the power command into a PV voltage command V_{cmd} as described in Section III. The V_{PV} voltage controller regulates the PV voltage by sending the d-axis current command, i_d, as in [39]. The inverter's output current is controlled in the dc–ac controller block using sinusoidal pulsewidth modulation with independent proportional-integral (PI) control on the d-axis and q-axis currents in the rotating synchronous (dq) reference frame, as in [39]. Reactive power output can be controlled separately by regulating the q-axis current command i_q in the voltage regulation block, but that is not the focus here.

The prototype inverter was connected to a real 5.28 kW PV array consisting of 48 Solarex 110S modules. An SMA SB3000 PV inverter operating in MPPT mode was connected to another Solarex 110S PV array with identical azimuth and orientation consisting of 26 modules. The two arrays were 10 m apart and used identical mounting methods, so they experienced nearly identical temperature and irradiance profiles. Thus, by operating the prototype inverter and the SMA inverter simultaneously, the MPPE method could be quantitatively validated.

An irradiance sensor based on a reference PV cell was mounted in the plane of the PV arrays to provide measurement of irradiance. As an alternative, it may be possible to use an online estimate of irradiance as described in [40] to reduce cost. A PV module temperature sensor mounted on the back of one of the modules provided a measurement of temperature. These irradiance and temperature measurements are used in the MPPE controller and the RAPC controller. The desired reserve power P_{RES}, provided externally based on economic and operational considerations, is subtracted from the maximum power estimate P_{MPPE} provided by the MPPE controller to generate a steady state operating power, P_{SET}. The power needed for frequency regulation, P_{FR}, is added to P_{SET} to generate the power command, P_{cmd}. The RAPC controller, described in Section III, converts the power command into a dc voltage command, V_{cmd}.

Fig. 5 shows recorded powers from the two inverters over a 3.6-h period on a partly cloudy day with significant changes in irradiance and temperature. The prototype inverter (Inverter 1) was operated in MPPE mode with a reserve power of 500 W (0.1 pu), and the SMA inverter (Inverter 2) was operated in MPPT mode. The yellow trace shows the maximum power estimate, P_{MPPE}, and the blue trace shows P_{AC1}, the output power of the prototype inverter. The purple trace shows the output power of the SMA inverter, P_{AC2}. Because the SMA inverter is powered by fewer Solarex PV modules than the prototype inverter, the power traces in Fig. 5 are all shown on a per-unit basis with the nominal power levels of

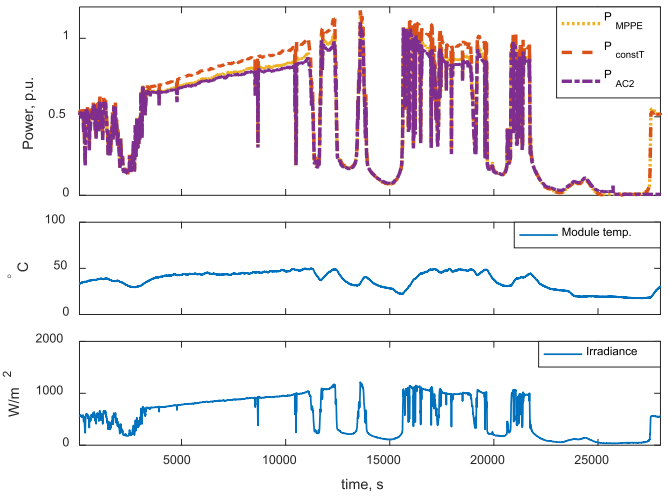

Fig. 6. Comparison of the MPPE method proposed here to a simpler method of estimation based on measured irradiance only.

the respective PV arrays as the power bases. Thus P_{MPPE} and P_{AC2} can be directly compared to validate the MPPE method. P_{MPPE} and P_{AC2} are nearly equal, as desired, with some small deviation evident at high-power levels. The desired reserve power of 0.1 pu is continuously maintained despite the challenging conditions of large changes in irradiance and temperature. This and other similar tests showed the MPPE method to be accurate and reliable over the expected range of operating conditions.

Fig. 6 shows a comparison of the MPPE method proposed here to a simpler method using only irradiance and not temperature, similar to that used in [5], over an 8-h period. Again the baseline for comparison is the measured output power of the SMA inverter operating in MPPT mode, P_{AC2}, shown in the purple trace. The estimated maximum power from the MPPE method proposed here, P_{MPPE}, is shown in yellow, and an estimate with the PV module temperature measurement fixed at 30 °C, P_{constT}, is shown in red. It is evident that the full MPPE method is significantly more accurate than the constant-temperature method.

III. Rapid Active Power Control

While it is possible to adapt typical MPPT methods such as perturb and observe to track a power reference, such methods are relatively slow because they rely on a multistep process: first adjust the PV array operating point V_{PV}, then allow the system to stabilize, measure output power, and adjust V_{PV} again iteratively until the desired power level is reached. This section presents a novel method of very quickly translating an active power command into a dc voltage command in a single control step. That dc voltage command can be passed to a conventional dc voltage controller, such as the PI voltage controller implemented in the prototype inverter, as shown in Fig. 4. This RAPC method is advantageous for use with grid support services designed to mitigate frequency contingency events because speed of response can be directly related to mitigation effectiveness.

Because irradiance and temperature change constantly, the PV array voltage needed to achieve a given output power is unknown. The RAPC method proposed here incorporates

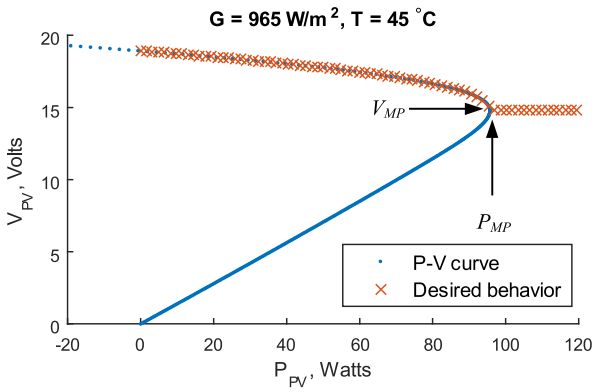

Fig. 7. Desired lookup table behavior for a fixed irradiance and temperature.

measurements of irradiance and module temperature to provide fast control of output power by predicting the V_{PV} value that will provide a commanded P_{PV}. As with the MPPE method, the RAPC method starts with PV module data sheet parameters and solves the I–V curve throughout the space of expected operating conditions. However, because low-order polynomial regression models for $V_{\mathrm{PV}}(P_{\mathrm{VP}}, G, T)$ resulted in poor fits [41], a 3-D lookup table (LUT) was generated instead. The LUT takes in P_{PV}, G, and T and interpolates between data points using trilinear interpolation to find the PV voltage V_{PV} that will produce the desired power at the measured irradiance and temperature. While a PV array power-voltage curve (Fig. 1) contains two voltages that will result in a given power, the LUT contains only the higher of the two voltages, which results in more easily-attained conversion ratios. For any $P_{\mathrm{cmd}} > P_{\mathrm{MP}}(G, T)$, the LUT returns $V_{\mathrm{MP}}(G, T)$.

The size of the LUT in each dimension was carefully considered with a goal of producing an accurate table with a tractable size. Because the LUT has three input dimensions, it can easily become very large. In the temperature and irradiance dimensions, the granularity of the LUT can be somewhat coarse because the gradients dV_{PV}/dT and dV_{PV}/dG are relatively smooth throughout the operating space. In contrast, the gradient $dV_{\mathrm{PV}}/dP_{\mathrm{PV}}$ is at times near zero but approaches (negative) infinity as V_{PV} approaches the maximum power voltage V_{MP}, as seen in Fig. 7. Thus the LUT requires a higher granularity in the P_{PV} dimension.

For any commanded power level greater than $P_{\mathrm{MP}}(G,T)$, the LUT should return $V_{\mathrm{MP}}(G,T)$, the voltage that will produce the maximum power available from the PV array. This desired behavior is illustrated by the red Xs in Fig. 7, which is based on a single Solarex 110S PV module. The red Xs also provide a visual indication of the LUT resolution needed in the P_{PV} dimension to accurately represent the PV array voltage-power characteristic in the vicinity of P_{MP}: Fig. 7 uses 100 evenly spaced power data points. One might conclude from Fig. 7 that the LUT could be designed to have high resolution only near the MPP, with lower resolution in other regions. However, as irradiance and temperature change, the location of the MPP varies widely. Thus the LUT should have fairly high granularity across all power operating points.

The lookup table data is generated by solving the five-parameter PV array model [32] at various operating points.

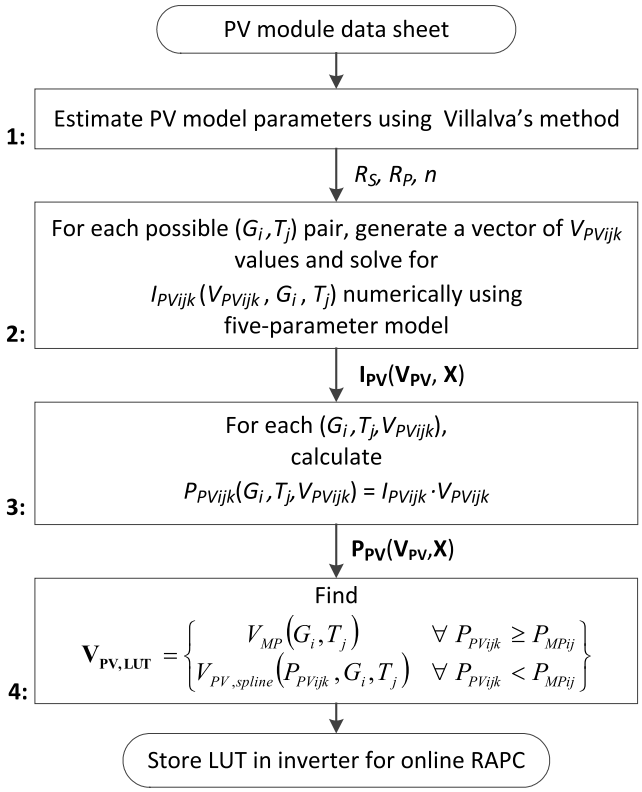

Fig. 8. Process for generating a lookup table for use in RAPC of PV.

The process for generating the LUT is summarized in Fig. 8.

Like the MPPE equation generation process, the process for generating RAPC LUT is performed once offline using only PV module data sheet values, and the LUT is stored in the inverter controller for online use. The process contains four steps. The first two steps in the LUT generation process are identical to the first two steps of the process for finding the regression coefficients for MPPE, as described in Section II. They result in I–V curves for all (G,T) pairs expected to be encountered in the field.

In the third step of the LUT generation process, the power P_{PV} at each operating point is calculated by multiplying I_{PV} by V_{PV}. The result of this process is a three dimensional array of powers P_{PV} for any given irradiance, module temperature, and voltage.

In the fourth and final step, the $P_{\mathrm{PV}}(V_{\mathrm{PV}}, G, T)$ data from Step 3 is interpolated using cubic splines to produce $V_{\mathrm{PV}}(P_{\mathrm{PV}}, G, T)$ values. Only the data for voltages greater than or equal to the maximum power voltage V_{MP} are used in the cubic spline interpolation. For all power commands greater than the maximum power for a given irradiance and temperature, the LUT returns V_{MP}. This is expressed mathematically as

$$\mathbf{V_{PV,LUT}} = \begin{Bmatrix} V_{\mathrm{MP}}(G_i, T_j) & \forall P_{\mathrm{PV}ijk} \geq P_{\mathrm{MP}ij} \\ V_{\mathrm{PV,spline}}(P_{\mathrm{PV}ijk}, G_i, T_j) & \forall P_{\mathrm{PV}ijk} < P_{\mathrm{MP}ij} \end{Bmatrix}. \tag{4}$$

As in Section II, the subscripts i, j, and k represent the indices of vectors of irradiance, module temperature, and voltage, respectively. $V_{\mathrm{MP}}(G_i, T_j)$ is the voltage that will produce maximum power for a given irradiance G_i and temperature T_j,

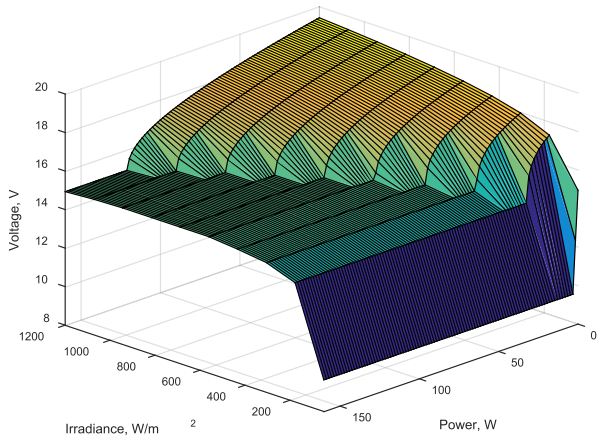

Fig. 9. RAPC lookup table surface at constant $T = 42$ °C with 10 data points in the irradiance dimension.

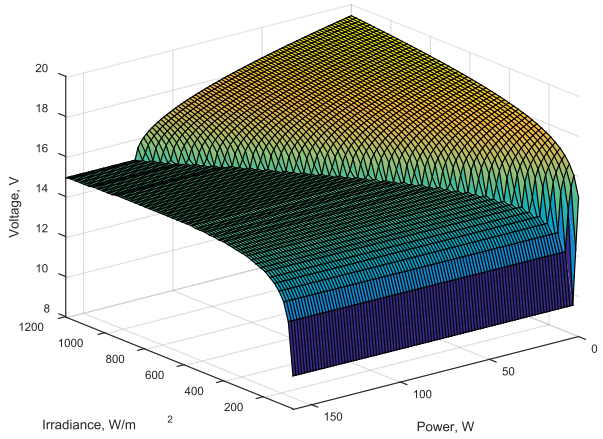

Fig. 10. RAPC lookup table surface at constant $T = 42$ °C with 50 data points in the irradiance dimension.

$V_{\mathrm{PV,spline}}$ is generated from cubic spline interpolation of the $\mathbf{P_{PV}}$ array onto 100 evenly spaced voltage points. MATLAB's spline() function was used to perform the interpolation here. The result is a 3-D array $\mathbf{V_{PV,LUT}}$ spanning all possible values of power, irradiance, and module temperature in the operating space.

As implemented here, the LUT is generated for a single PV module. Hence the input power command to the LUT, P_{LUT}, is scaled down from the measured power by dividing by the number of PV modules in the array, N (i.e., $P_{\mathrm{LUT}} = P_{\mathrm{cmd}}/N$), and the output voltage from the LUT, V_{LUT}, is scaled up by multiplying by the number of modules in each series string, N_S (i.e., $V_{\mathrm{cmd}} = V_{\mathrm{LUT}} \cdot N_S$).

The LUT size in the G dimension can be selected by visually inspecting plots of the LUT at fixed T and selecting a number of irradiance data points that eliminates artifacts. Fig. 9 shows a surface of the LUT at $T = 42$ °C with 10 data points in G, with notable artifacts near the maximum power region (the crease in the surface). In Fig. 10, the resolution in G has been increased by a factor of five, and the surface is now smooth, as desired. A similar process was used to select the LUT size in the T dimension, as seen in [41]. Fifty irradiance data points and 30 temperature data points were used in the final LUT implemented here. Thus the final

LUT as implemented in the experimental validation below contains $30 \cdot 50 \cdot 100 = 150\,000$ data points, requiring about 0.6 MB of memory if implemented using single-precision floating point data. This size is within the capacity of many modern microcontrollers but could likely be reduced through further optimization if desired.

Non-idealities such as PV module mismatch, soiling, and non-uniformities in temperature and irradiance will inevitably introduce some small but acceptable error in this RAPC method. Future work will look at ways to reduce this error, as briefly discussed in the conclusions. The costs of the irradiance and temperature sensors would add roughly 3% to the cost of a 5 kW residential PV installation. PV arrays that experience partial shading for significant portions of the day would not be good candidates for the MPPE and RAPC methods presented here.

IV. RAPC Experimental Validation

The RAPC method described above was implemented in the same prototype PV inverter (Fig. 4) as in Section II and supplied from the same 5.28 kW PV array. The frequency regulation block in Fig. 4 was programmed with a 5% droop slope. This means that a frequency change equal to 5% of the nominal frequency, or 3 Hz, will result in a change of 100% of the inverter's nominal power, so $P_{\mathrm{FR}} = P_0 \cdot (f - f_0)/(f_0 \cdot 0.05)$, where P_0 is the rated inverter power, f is the measured grid frequency from the PLL, and $f_0 = 60$ Hz. A 5% droop slope is a common value used in synchronous machines, though machine droop response is orders of magnitude slower than the inverter responses shown below. The programmed droop slope did not contain a deadband, as is common with conventional generators, but it could easily be modified to incorporate a deadband. A controllable ac power supply was used to produce frequency events, and the inverter's response was recorded, including internal control signals. While the speed of a control response would typically be evaluated using step changes in the input variable, step changes in frequency do not occur on power systems containing synchronous generation due to generator inertia. Hence the test events were designed to mimic worst case real events in magnitude and rate of change of frequency (ROCOF). Smaller interconnected ac power systems tend to have more severe frequency events, both in magnitude and in ROCOF. For example, in studies that simulated a separation of the Ireland and Northern Ireland electrical systems, a ROCOF of over 1 Hz/s was observed in Ireland, and a ROCOF of over 2 Hz/s was observed in Northern Ireland [42]. In terms of magnitude, a frequency event with a minimum frequency (nadir) of 59 Hz would be considered a very large event in the continental U.S., but on the most populous Hawaiian island of Oahu, such events have occurred more than once per year in recent years. Overfrequency events tend to be less severe in terms of both magnitude and ROCOF. Faster events are more challenging from an inverter control perspective in terms of phase-locked loop (PLL) response and dc voltage controller response. The frequency events used in the tests below were selected based on these considerations.

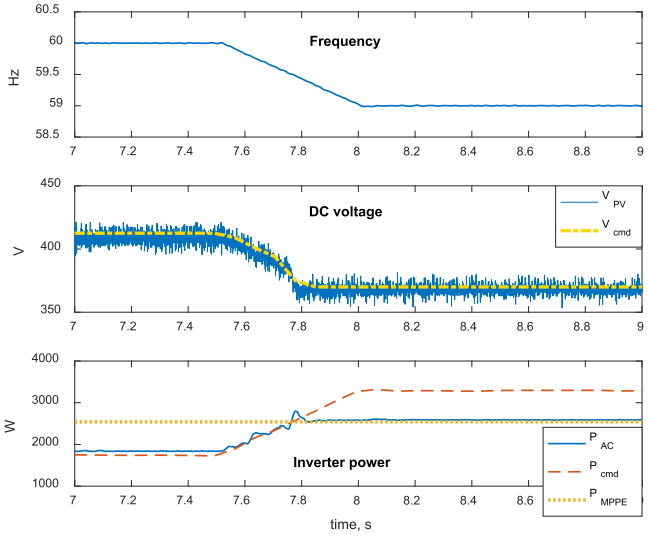

Fig. 11. RAPC response to a frequency event with a nadir of 59 Hz and a 2 Hz/s ROCOF, with 0.8 kW of reserve power.

Fig. 11 shows the prototype inverter's response to a frequency event with a nadir of 59 Hz and a ROCOF of 2 Hz/s, faster than what would be seen on larger interconnected power systems but possible for a smaller system such as Ireland's. The inverter was operating in MPPE mode with 0.8 kW of power in reserve and a 5% droop. The inverter begins responding to the frequency event almost immediately. Both the measured dc voltage V_{PV} and the measured ac power P_{AC} track closely their respective commanded values, V_{cmd} and P_{cmd}. The high frequency component of the dc voltage measurement is a combination of measurement noise, switching frequency ripple, and dc voltage ripple at a multiple of the line frequency (likely due to a slight imbalance between phases). The measured power lags the commanded power by less than 20 ms. Note that P_{cmd} exceeds P_{MPPE} in Fig. 11 because the desired frequency regulation power P_{FR} exceeds the reserve power P_{RES}. Allowing P_{cmd} to exceed P_{MPPE} in these situations prevents an underestimate in P_{MPPE} from directly limiting the power command; when P_{cmd} is greater than the maximum available power, as in the right-hand portion of Fig. 11, the RAPC controller targets the PV array's maximum power voltage. This results in maximum available output power, the desired response for this scenario.

The inverter's response to an underfrequency event with a very fast ROCOF of 6 Hz/s is shown in Fig. 12. This high ROCOF represents a simulated future event on the Irish grid with a significantly higher proportion of inverter-coupled generation, leading to lower system inertia [42]. This likely represents the fastest ROCOF that may be seen on a bulk power system. Such a fast event is challenging for an inverter to respond to from the perspective of PLL and voltage control design. The inverter was again programmed with a 5% droop slope, and a reserve power of 0.8 kW. The inverter responds well, reaching the new power within 4.5 line cycles. However, the limitations of the inverter's response become evident. There is visible overshoot and some ringing in P_{AC} and V_{PV} as the voltage controller does not to track the relatively fast-changing RAPC voltage commands perfectly. Similar but

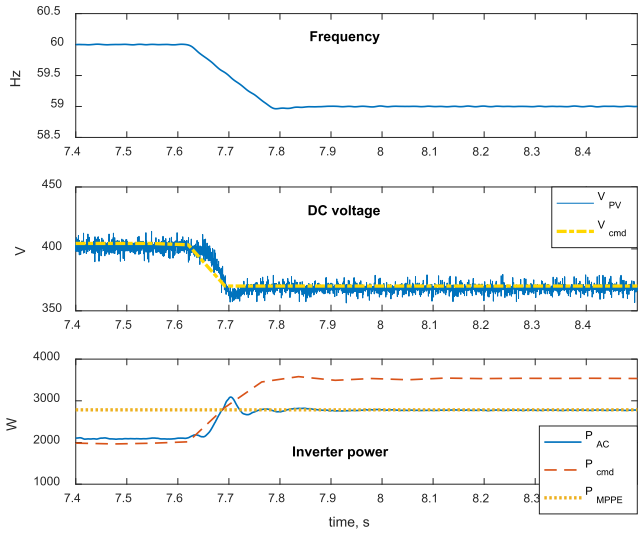

Fig. 12. RAPC response to a very fast frequency event with a nadir of 59 Hz and a 6 Hz/s ROCOF, with 0.8 kW of reserve power.

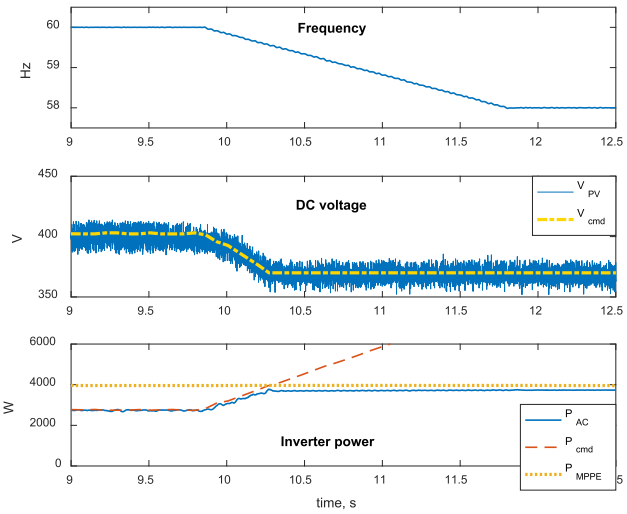

Fig. 13. RAPC response of the prototype inverter to a frequency event with a lower nadir of 58 Hz and a 1 Hz/s ROCOF.

smaller effects can be seen in Figs. 11 and 13. Note that the dc capacitor in this inverter is larger than typical for an inverter of this size for historical reasons unrelated to this control scheme, so a given variation in dc voltage produces a larger change in P_{AC}. The oscillations are not large in magnitude relative to the response and they die out quickly, so it is expected that such a response would still be effective in mitigating the frequency event, but they do indicate that this high-ROCOF event is near the edge of the inverter's response capability. These experiments used an inverter with a conventional voltage controller to demonstrate the compatibility of RAPC with conventional controls. However, it will likely be possible to improve the bandwidth of this early prototype without compromising control stability by optimizing the PLL and voltage controller design.

Some power systems experience frequency events that are larger in magnitude than those shown above. For example, some contingency events measured on the island of Oahu have had nadirs below 58.5 Hz and ROCOFs close to 1 Hz/s. The response of the inverter to a test representing such an event is shown in Fig. 13. The inverter had a reserve power of 1.2 kW (0.25 pu) and a more aggressive droop slope of 3%, representing the steeper end of the range of droop slopes typically used in synchronous machines. Recall that droop slope is defined as the percentage change in frequency that leads to a change in generator power of 100% of the unit's rating, so a smaller droop slope leads to a more aggressive response. Again the inverter's response is fast and accurate. Note that due to the steepness of the droop slope and the magnitude of the event, the power command goes much higher than the inverter's rating. Thus the effect of the higher droop slope in this case is to deploy the PV system's reserves faster, rather than to change the maximum power reached.

During each of the above events, the error in measured power (as a percent of PV system rating) remains under 2% in steady state and under 6% during transients.

V. Conclusion

The RAPC method introduced here has been experimentally shown to provide very fast and accurate response to a demanding range of grid frequency events. The experimental validation used two real PV arrays to demonstrate that the method is robust to realistic changes in weather conditions. Used in conjunction with a PV MPPE method experimentally validated here, the RAPC method enables a suite of fast-responding PV inverter APC methods, including but not limited to the fast power-frequency droop response demonstrated here.

The experimental results presented here were recorded at a 5 kW scale, but the MPPE and RAPC control methods are expected to scale well to very large systems. In a typical utility-scale PV plant consisting of many inverters, accurate MPPE and RAPC results will be achieved if each inverter uses irradiance and module temperature measurements from its own PV array, so additional sensors will be needed.

The nonidealities inherent in PV arrays in the field such as module mismatch, soiling, and nonuniform aging will lead to some loss of accuracy of the RAPC method described here. In the future work, the steady-state accuracy of RAPC can be improved without loss of control speed by adding a slower control loop to regulate power to its commanded value after the initial fast response. Such an outer control loop could also allow the size of the RAPC lookup table to be reduced if desired. It should also be possible to use machine learning techniques to continuously update the RAPC table in the inverter based on operational data.

There has been little incentive in the past for grid-interactive PV inverters to have particularly high-bandwidth PLLs or dc voltage controllers. However, for emerging applications such as RAPC, the experimental results presented here suggest it may be beneficial to design faster low-level controls, allowing still faster response to frequency events or other grid disturbances.

References

[1] P. Kundur, *Power System Stability and Control*. New York, NY, USA: McGraw-Hill, 1994.

[2] *Frequency Regulation Compensation in the Organized Wholesale Power Markets*, document FERC Order 755, U.S. Federal Energy Regulatory Commission (FERC), Oct-2011.

[3] *Third-Party Provision of Primary Frequency Response Service*, document FERC Order 819, Federal Energy Regulatory Commission, Nov. 2015.
[4] *Hawaiian Electric Companies' PSIP Update Report: Book 2 of 2*, document PUC Docket 2014-0183, The Hawaiian Electric Companies, Apr. 2016.
[5] V. Gevorgian and B. O'Neill, "Advanced grid-friendly controls demonstration project for utility-scale PV power plants," NREL, Golden, CO, USA, Tech. Rep. NREL/TP-5D00-65368, Jan. 2016.
[6] P. M. S. Carvalho, P. F. Correia, and L. A. F. M. Ferreira, "Distributed reactive power generation control for voltage rise mitigation in distribution networks," *IEEE Trans. Power Syst.*, vol. 23, no. 2, pp. 766–772, May 2008.
[7] *Standard for Interconnecting Distributed Resources With Electric Power Systems—Amendment 1*, IEEE Standard 1547a-2014, 2014.
[8] *Minimum Technical Requirements for Photovoltaic Generation (PV) Projects*, Puerto Rico Electr. Power Authority, San Juan, PR, USA, Nov. 2011.
[9] B.-I. Craciun, T. Kerekes, D. Sera, and R. Teodorescu, "Frequency support functions in large PV power plants with active power reserves," *IEEE J. Emerg. Sel. Topics Power Electron.*, vol. 2, no. 4, pp. 849–858, Dec. 2014.
[10] *Electricity Storage Technology Brief*, Int. Energy Agency Energy Technol. Syst. Anal. Programme (IEA-ETSAP) and Int. Renew. Energy Agency (IRENA), Masdar, Abu Dhabi. Apr. 2012.
[11] A. Hoke and D. Maksimović, "Active power control of photovoltaic power systems," in *Proc. 1st IEEE Conf. Technol. Sustain. (SusTech)*, Aug. 2013, pp. 70–77.
[12] *Technical Regulation 3.2.2 for PV Power Plants With a Power Output Above 11 kW*, Energinet.dk, Erritsø, Denmark, 2015.
[13] *Oahu Distributed PV Grid Stability Study—Part 1: System Frequency Response to Generator Contingency Events*, GE Energy Consulting, Schenectady, NY, Mar. 2016.
[14] P. Rodriguez, A. V. Timbus, R. Teodorescu, M. Liserre, and F. Blaabjerg, "Flexible active power control of distributed power generation systems during grid faults," *IEEE Trans. Ind. Electron.*, vol. 54, no. 5, pp. 2583–2592, Oct. 2007.
[15] M. Datta, T. Senjyu, A. Yona, T. Funabashi, and C.-H. Kim, "A frequency-control approach by photovoltaic generator in a PV–diesel hybrid power system," *IEEE Trans. Energy Convers.*, vol. 26, no. 2, pp. 559–571, Jun. 2011.
[16] V. A. K. Pappu, B. Chowdhury, and R. Bhatt, "Implementing frequency regulation capability in a solar photovoltaic power plant," in *Proc. North Amer. Power Symp. (NAPS)*, 2010, pp. 1–6.
[17] L. D. Watson and J. W. Kimball, "Frequency regulation of a microgrid using solar power," in *Proc. 26th Annu. IEEE Appl. Power Electron. Conf. Expo. (APEC)*, Mar. 2011, pp. 321–326.
[18] A. F. Okou, O. Akhri, R. Beguenane, and M. Tarbouchi, "Nonlinear control strategy insuring contribution of PV generator to voltage and frequency regulation," in *Proc. 6th IET Int. Conf. Power Electron., Mach. Drives (PEMD)*, 2012, pp. 1–5.
[19] P. P. Zarina, S. Mishra, and P. C. Sekhar, "Deriving inertial response from a non-inertial PV system for frequency regulation," in *Proc. IEEE Int. Conf. Power Electron., Drives Energy Syst. (PEDES)*, Dec. 2012, pp. 1–5.
[20] J. Neely, J. Johnson, J. Delhotal, S. Gonzalez, and M. Lave, "Evaluation of PV frequency-watt function for fast frequency reserves," in *Proc. Appl. Power Electron. Conf.*, 2016, pp. 1926–1933.
[21] H. Shi, F. Zhuo, H. Yi, F. Wang, D. Zhang, and Z. Geng, "A novel real-time voltage and frequency compensation strategy for photovoltaic-based microgrid," *IEEE Trans. Ind. Electron.*, vol. 62, no. 6, pp. 3545–3556, Jun. 2015.
[22] A. Sangwongwanich, Y. Yang, and F. Blaabjerg, "Sensorless reserved power control strategy for two-stage grid-connected photovoltaic systems," in *Proc. IEEE 7th Int. Symp. Power Electron. Distrib. Generat. Syst. (PEDG)*, Jun. 2016, pp. 1–8.
[23] A. Hoke, E. Muljadi, and D. Maksimovic, "Real-time photovoltaic plant maximum power point estimation for use in grid frequency stabilization," in *Proc. IEEE 16th Workshop Control Modeling Power Electron. (COMPEL)*, Jul. 2015, pp. 1–7.
[24] H. Xin, Z. Lu, Y. Liu, and D. Gan, "A center-free control strategy for the coordination of multiple photovoltaic generators," *IEEE Trans. Smart Grid*, vol. 5, no. 3, pp. 1262–1269, May 2014.
[25] M. C. Chandorkar, D. M. Divan, and R. Adapa, "Control of parallel connected inverters in standalone AC supply systems," *IEEE Trans. Ind. Appl.*, vol. 29, no. 1, pp. 136–143, Jan./Feb. 1993.
[26] F. Teng and G. Strbac, "Evaluation of synthetic inertia provision from wind plants," in *Proc. IEEE Power Energy Soc. General Meeting*, Jul. 2015, pp. 1–5.
[27] J. Matevosyan, "Future ancillary services developments in ERCOT," presented at the IEEE PES General Meeting, National Harbor, MD, USA, Jul. 2014.
[28] J. C. Vasquez, R. A. Mastromauro, J. M. Guerrero, and M. Liserre, "Voltage support provided by a droop-controlled multifunctional inverter," *IEEE Trans. Ind. Electron.*, vol. 56, no. 11, pp. 4510–4519, Nov. 2009.
[29] A. Marinopoulos, F. Papandrea, M. Reza, S. Norrga, F. Spertino, and R. Napoli, "Grid integration aspects of large solar PV installations: LVRT capability and reactive power/voltage support requirements," in *Proc. IEEE Trondheim PowerTech*, Jun. 2011, pp. 1–8.
[30] B. Subudhi and R. Pradhan, "A comparative study on maximum power point tracking techniques for photovoltaic power systems," *IEEE Trans. Sustain. Energy*, vol. 4, no. 1, pp. 89–98, Jan. 2013.
[31] M. A. G. de Brito, L. Galotto, L. P. Sampaio, G. E. de Azevedo e Melo, and C. A. Canesin, "Evaluation of the main MPPT techniques for photovoltaic applications," *IEEE Trans. Ind. Electron.*, vol. 60, no. 3, pp. 1156–1167, Mar. 2013.
[32] M. G. Villalva, J. R. Gazoli, and E. R. Filho, "Comprehensive approach to modeling and simulation of photovoltaic arrays," *IEEE Trans. Power Electron.*, vol. 24, no. 5, pp. 1198–1208, May 2009.
[33] Y. Mahmoud and E. F. El-Saadany, "A photovoltaic model with reduced computational time," *IEEE Trans. Ind. Electron.*, vol. 62, no. 6, pp. 3534–3544, Jun. 2015.
[34] C. R. Osterwald, J. Adelstein, J. A. del Cueto, B. Kroposki, D. Trudell, and T. Moriarty, "Comparison of degradation rates of individual modules held at maximum power," in *Proc. Conf. Rec. IEEE 4th World Conf. Photovolt. Energy Convers.*, vol. 2. May 2006, pp. 2085–2088.
[35] S. Anand, S. K. Gundlapalli, and B. G. Fernandes, "Transformer-less grid feeding current source inverter for solar photovoltaic system," *IEEE Trans. Ind. Electron.*, vol. 61, no. 10, pp. 5334–5344, Oct. 2014.
[36] W. Li, Y. Gu, H. Luo, W. Cui, X. He, and C. Xia, "Topology review and derivation methodology of single-phase transformerless photovoltaic inverters for leakage current suppression," *IEEE Trans. Ind. Electron.*, vol. 62, no. 7, pp. 4537–4551, Jul. 2015.
[37] S. Rivera, B. Wu, R. Lizana, S. Kouro, M. Perez, and J. Rodriguez, "Modular multilevel converter for large-scale multistring photovoltaic energy conversion system," in *Proc. IEEE Energy Convers. Congr. Expo.*, Sep. 2013, pp. 1941–1946.
[38] W. Kramer, S. Chakraborty, M. Shirazi, B. Lundstrom, and K. Harrison, "Advanced power electronics interface initiative: Smart grid and advanced power electronics research and development," California Energy Commission, Tech. Rep. CEC-500-2014-006, Sacramento, CA, Jun. 2012.
[39] S. Buso and P. Mattavelli, *Digital Control in Power Electronics*. San Rafael, CA, USA: Morgan & Claypool, 2006.
[40] M. Carrasco, F. Mancilla-David, and R. Ortega, "An estimator of solar irradiance in photovoltaic arrays with guaranteed stability properties," *IEEE Trans. Ind. Electron.*, vol. 61, no. 7, pp. 3359–3366, Jul. 2014.
[41] A. F. Hoke, "Active power control of photovoltaic systems, and electric vehicle optimization including the costs of battery degradation," Ph.D. dissertation, Dept. Elect. Eng., Univ. Colorado, Boulder, CO, USA, 2016.
[42] *Rate of Change of Frequency (ROCOF): Review of TSO and Generator Submissions—Final Report*, PPA Energy, Guildford, U.K., May 2013.

Anderson F. Hoke (M'15) received the B.A. degree in engineering physics from Dartmouth College, Hanover, NH, USA, in 2001, and the M.S. and Ph.D. degrees in electrical engineering from the University of Colorado, Boulder, CO, USA, in 2013 and 2016, respectively.

He was a Graduate Research Participant at the National Renewable Energy Laboratory (NREL), Golden, CO, USA, and a Research Assistant at the Colorado Power Electronics Center, University of Colorado, from 2010 to 2014. In 2014, he joined the Power Systems Engineering Center, NREL, as a Research Engineer. He has co-authored over 30 publications. His current research interests include power electronics for integration of distributed and renewable energy with electric power systems.

Dr. Hoke was a recipient of the IEEE Power and Energy Society General Meeting Best Conference Paper Award in 2015. He is a registered Professional Engineer in the state of Colorado.

Mariko Shirazi (M'10) received the B.S. degree in mechanical engineering from the University of Alaska, Fairbanks, AK, USA, in 1996, and the M.S. and Ph.D. degrees in electrical engineering from the University of Colorado, Boulder, CO, USA, in 2007 and 2009, respectively.

From 1996 to 2004, she was an Engineer at the National Wind Technology Center, National Renewable Energy Laboratory (NREL), Golden, CO, USA, where she was involved in the design and deployment of hybrid wind-diesel power systems for village power applications. From 2009 to 2013, she was with the Power Systems Engineering Center, NREL, where she was involved in designing and building of power electronics for PV-battery-diesel hybrid power systems. From 2013 to 2015, she was assigned to NREL's Energy Systems Integration Facility to assist with the design and commissioning of the facility. She re-joined with the Power Systems Engineering Center, NREL, in 2015. Her current research interests include the design and control of power converters for microgrid applications.

Sudipta Chakraborty (M'07–SM'13) received the B.E. degree in electrical engineering from Bengal Engineering College (now Indian Institute of Engineering Science and Technology, Shibpur), Howrah, India, in 2001, and the Ph.D. degree in engineering systems and electrical specialty from the Colorado School of Mines, Golden, CO, USA, in 2007.

He is currently a Principal Electrical Engineer at the National Renewable Energy Laboratory, Golden. He has co-edited a book titled *Power Electronics for Renewable and Distributed Energy Systems: A Sourcebook of Topologies, Control, and Integration* (Springer-Verlag), in 2013. His current research interests include power electronics and grid integration of renewable and distributed energy resources to the electric grid.

Dr. Chakraborty is the Chair of the IEEE 1547.1 full-revision working group.

Eduard Muljadi (M'82–SM'94–F'10) received the Ph.D. degree in electrical engineering from the University of Wisconsin–Madison, Madison, WI, USA.

From 1988 to 1992, he was with California State University at Fresno, Fresno, CA, USA. In 1992, he joined the National Renewable Energy Laboratory, Golden, CO, USA. He holds two patents in power conversion for renewable energy. His current research interests include the fields of electric machines, power electronics, and power systems in general with an emphasis on renewable energy applications.

Dr. Muljadi is a member of Eta Kappa Nu and Sigma Xi, and an Editor of the IEEE TRANSACTIONS ON ENERGY CONVERSION. He is involved in the activities of the IEEE Industry Application Society (IAS), the Power Electronics Society, and the Power and Energy Society (PES). He is currently a member of various committees of the IAS, and the Working Group on Renewable Technologies and the Task Force on Dynamic Performance of Wind Power Generation, both of the PES.

Dragan Maksimovic (M'89–SM'04–F'15) received the B.S. and M.S. degrees in electrical engineering from the University of Belgrade, Belgrade, Serbia, in 1984 and 1986, respectively, and the Ph.D. degree from the California Institute of Technology, Pasadena, CA, USA, in 1989.

From 1989 to 1992, he was with the University of Belgrade. Since 1992, he has been with the Department of Electrical, Computer, and Energy Engineering, University of Colorado, Boulder, CO, USA, where he is currently a Professor and Co-Director with the Colorado Power Electronics Center. He has co-authored over 250 publications and the textbook *Fundamentals of Power Electronics*. His current research interests include power electronics for renewable energy sources and energy efficiency, high-frequency power conversion using wide bandgap semiconductors, digital control of switched-mode power converters, as well as analog, digital, and mixed-signal integrated circuits for power management applications.

Prof. Maksimovic was a receipient of the 1997 NSF CAREER Award, the IEEE PELS Transactions Prize Paper Awards in 1997 and 2016, the IEEE PELS Prize Letter Awards in 2009 and 2010, the University of Colorado Inventor of the Year Award in 2006, the IEEE PELS Modeling and Control Technical Achievement Award for 2012, the Holland Excellence in Teaching Awards in 2004 and 2011, the Charles Hutchinson Memorial Teaching Award for 2012, and the 2013 Boulder Faculty Assembly Excellence in Teaching Award.